COMMUNICATIONS IN COMPUTATIONAL PHYSICS
Vol. 3, No. 1, pp. 160-179

Commun. Comput. Phys.
January 2008

Advanced Computational Methods of Rapid and Rigorous 3-D Inversion of Airborne Electromagnetic Data

Leif H. Cox[1] and Michael S. Zhdanov[2,*]

[1] *Department of Geophysical Engineering, Montana Tech of the University of Montana, 1300 W Park Street, Butte, MT 59701 -8997, USA.*
[2] *Department of Geology and Geophysics, University of Utah, 135 S. 1460 E. Rm 719, Salt Lake City, UT 84112, USA.*

Received 19 October, 2006; Accepted (in revised version) 6 June, 2007

Available online 14 September 2007

Abstract. We develop a new computational method for modeling and inverting frequency domain airborne electromagnetic (EM) data. Our method is based on the contraction integral equation method for forward EM modeling and on inversion using the localized quasi-linear (LQL) approximation followed by the rigorous inversion, if necessary. The LQL inversion serves to provide a fast image of the target. These results are checked by a rigorous update of the domain electric field, allowing a more accurate calculation of the predicted data. If the accuracy is poorer than desired, rigorous inversion follows, using the resulting conductivity distribution and electric field from LQL as a starting model. The rigorous inversion iteratively solves the field and domain equations, converting the non-linear inversion into a series of linear inversions. We test this method on synthetic and field data. The results of the inversion are very encouraging with respect to both the speed and the accuracy of the algorithm, showing this is a useful tool for airborne EM interpretation.

AMS subject classifications: 86A22, 86A25, 86A60

Key words: Computational geophysics, airborne, electromagnetics, inversion, 3-D, LQL, rigorous.

1 Introduction

Modern computational methods have become widely used in exploration geophysics. For many years, the basic model for interpretation in electromagnetic (EM) geophysics was a one-dimensional (1-D) model of a layered earth or a two-dimensional (2-D) model with the resistivity varying with the depth and along the profile of observation only.

*Corresponding author. *Email addresses:* lcox@mtech.edu (L. H. Cox), mzhdanov@mines.utah.edu (M. S. Zhdanov)

However, in recent years geophysicists more often use full three-dimensional (3-D) models for interpretation of practical data. This requires developing the corresponding mathematical methods of interpretation, based on the modern achievements of EM theory and advanced computational methods of modeling and inversion. To date, this has not been successfully accomplished for airborne electromagnetic data (AEM). In this paper we will demonstrate how the recent advances in 3-D numerical modeling and inversion of EM data help in developing effective methods for 3-D interpretation of AEM geophysical data.

A typical frequency domain airborne EM survey is based on the same principles as a ground inductive EM survey. In the airborne case, several transmitter and receiver coils are attached to an aircraft. There are several configurations, but typically the transmitter-receiver pairs are housed in a 'bird' towed behind the aircraft. The platform flies over the survey area towing this bird and continuously transmits an electromagnetic field with specific frequencies excited by transmitter coils. The EM field propagates into the ground and reaches some geoelectrical target such as an ore body. The electric currents induced in the ground and within the anomalous body generate a secondary electromagnetic field. The receiver coils measure the total EM field (a superposition of the primary field generated by the transmitter and the secondary EM field) at the bird's location. The goal of the survey is to find the location and electrical parameters of the underground geoelectrical formations. Note that the typical airborne EM system has several transmitter-receiver pairs. For example, typical AEM systems have transmitter-receiver pairs forming coplanar arrays, where both the transmitter and receiver coils of which can transmit/measure the vertical components of the EM field only, and coaxial arrays, with the transmitter and receiver coils transmiting/measuring the horizontal components of the EM field only.

The airborne platform creates a very powerful tool for surveying large areas rapidly and relatively inexpensively. Surveys may cover thousands of line kilometers with multi-component and multi-frequency soundings every few meters. This enables collecting a huge amount of data about the electrical properties of the earth. However, interpreting the massive amounts of data gathered poses a significant challenge. Any 3-D inversion must discretize the earth into thousands of cells representing the conductivity distribution. Computationally, this problem is exacerbated by the fact that for each sounding point and channel, a new electric field is introduced into the earth. This requires solving a large number of equations simultaneously for a full rigorous inversion.

These problems have been addressed in the past by attacking one single sounding location at a time and assuming a 1-D earth, usually with conductivity depth transforms (CDT) [6, 11, etc.] or layered earth inversions (LEI) (e.g., [2]). The CDT methods are extremely fast, but do not model the earth correctly in the sense that the theoretical EM response for one dimensional earth recovered does not necessarily fit the observed data. LEIs, while significantly slower than CDTs, produce the correct response of a 1-D layered earth. Yet they do not take into account the true three dimensional nature of the subsurface. As shown by [1], even when the predicted 1-D model response is within a few percent of the observed data, the resulting conductivity model may be a poor approxi-

mation of the true model.

Over the last several years, the Consortium for Electromagnetic Modeling and Inversion (CEMI) has developed methods and the corresponding software to quantitatively interpret AEM data in 3-D. These methods are based on the localized quasi-linear (LQL) approximation [15, 18]. This method provides a fast algorithm for 3-D imaging of conductive targets. It can be treated as an effective reconnaissance tool, or accurate inversion in the case of low conductivity contrasts. However, when this condition is not met, the recovered conductivity of the target may be significantly underestimated, and the shape of the inverse images may be distorted in comparison with the true model.

In the current paper, we attempt to overcome this limitation of the LQL method by considering a more rigorous forward modeling technique in the framework of the regularized inversion scheme. According to this approach, the solution of the AEM inverse problem is formulated using two sets of integral equations: 1) a field equation connecting the observed data in the receivers with the anomalous conductivity within the inversion domain; 2) a domain equation with respect to the electric field inside the anomalous domain. The main difficulty in the solution of these equations arises from the fact that, in the case of the AEM survey, we are dealing with multi-transmitter, multi-receiver data. This requires simultaneous analysis of as many pairs of the field and domain equations as we have transmitter positions. We solve a preconditioned form of the domain equation with the complex generalized minimum residual method (CGMRES) to ensure convergence of the domain equation. The field equation is solved using the re-weighted regularized conjugate gradient (RRCG) method.

2 Computation methods

2.1 Basic integral equations of EM modeling

For completeness, we begin our paper with the formulation of the basic principles of the integral electric (IE) equation.

We consider a 3-D geoelectrical model with a background (horizontally layered) conductivity σ_b and a local inhomogeneous region, D, with an arbitrarily varying conductivity $\sigma=\sigma_b+\Delta\sigma$. The magnetic permeability of the media is equal to the free-space magnetic permeability $\mu=\mu_0=4\pi\times10^{-7}$ Henry/meter. In the framework of the AEM method, one uses a moving transmitter-receiver system consisting of pairs of vertical magnetic dipoles (horizontal coplanar coil pairs) and pairs of horizontal magnetic dipoles (vertical coaxial coil pairs). A frequency domain EM field is generated by a transmitter dipole and is recorded by a receiver dipole. The goal is to find the anomalous conductivity distribution, $\Delta\sigma$, based on the data collected by the AEM survey.

We can represent the EM field in this model as a sum of the background and anomalous fields:

$$\mathbf{E}=\mathbf{E}^b+\mathbf{E}^a, \tag{2.1}$$

$$\mathbf{H}=\mathbf{H}^b+\mathbf{H}^a, \tag{2.2}$$

where the background field is generated by the given sources in the model with the background distribution of conductivity σ_b, and the anomalous field is produced by the anomalous conductivity distribution, $\Delta\sigma$.

According to the integral form of Maxwell's equations [14], the anomalous field in the frequency domain can be represented as an integral over the excess (anomalous) currents, $\mathbf{j}^a = \Delta\sigma\,\mathbf{E}$, in the inhomogeneous domain, D:

$$\mathbf{E}^a(\mathbf{r}_j) = \mathbf{G}_E(\Delta\sigma\mathbf{E}) = \iiint_D \widehat{\mathbf{G}}_E(\mathbf{r}_j\,|\,\mathbf{r})\,\Delta\sigma(\mathbf{r})\,\mathbf{E}(\mathbf{r})\,dv, \tag{2.3}$$

$$\mathbf{H}^a(\mathbf{r}_j) = \mathbf{G}_H(\Delta\sigma\mathbf{E}) = \iiint_D \widehat{\mathbf{G}}_H(\mathbf{r}_j\,|\,\mathbf{r})\,\Delta\sigma(\mathbf{r})\,\mathbf{E}(\mathbf{r})\,dv, \tag{2.4}$$

where $\widehat{\mathbf{G}}_{E,H}(\mathbf{r}_j\,|\,\mathbf{r})$ stands for the electric or magnetic Green's function defined for an unbounded conductive medium with normal conductivity σ_b. $\mathbf{G}_{E,H}(\mathbf{r}_j\,|\,\mathbf{r})$ is corresponding Green's tensor.

Eq. (2.4), which connects the observed magnetic field at the receivers with the electric field inside the anomalous domain, D, represents a *field equation*. Writing Eq. (2.3) for the points within the anomalous domain, $\mathbf{r}_j \in D$, we arrive at a *domain equation*.

2.2 Localized quasi-linear inversion background

We first solve the AEM inverse problem using the localized quasi-linear (LQL) method [18]. This method is based on the assumption that the anomalous field, $\mathbf{E}^a$, inside the inhomogeneous domain is linearly proportional to the background field, $\mathbf{E}^b$, through electrical reflectivity tensor, $\widehat{\boldsymbol{\lambda}}$, [16,17] which is assumed to be independent of the transmitter position:

$$\mathbf{E}^a_I(\mathbf{r}) \approx \widehat{\boldsymbol{\lambda}}(\mathbf{r}) \cdot \mathbf{E}^b_I(\mathbf{r}), \tag{2.5}$$

where $\mathbf{E}^a_I$ and $\mathbf{E}^b_I$ represent the anomalous and background electric fields at the I^{th} transmitter position. In the framework of the localized quasi-linear (LQL) approximation [14,18], it is assumed that the electrical reflectivity tensor, $\widehat{\boldsymbol{\lambda}}$, is source independent.

Substituting Eq. (2.5) into Eq. (2.1), the total electric field becomes:

$$\mathbf{E}_I = \mathbf{E}^b_I + \widehat{\lambda}\mathbf{E}^b_I = (\widehat{\mathbf{I}} + \widehat{\boldsymbol{\lambda}})\mathbf{E}^b_I. \tag{2.6}$$

Following [16,18], we introduce a new tensor function,

$$\widehat{\mathbf{m}}(\mathbf{r}) = \Delta\sigma_{LQL}(\mathbf{r})\left(\widehat{\mathbf{I}} + \widehat{\boldsymbol{\lambda}}(\mathbf{r})\right), \tag{2.7}$$

which we call a modified material property tensor.

Substituting Eq. (2.6) into Eqs. (2.3) and (2.4), and using (2.7), we can write:

$$\mathbf{E}^a_I(\mathbf{r}_j) = \mathbf{G}_E\left[\widehat{\mathbf{m}}(\mathbf{r}) \cdot \mathbf{E}^b_I(\mathbf{r})\right], \tag{2.8}$$

$$\mathbf{H}^a_I(\mathbf{r}_j) = \mathbf{G}_H\left[\widehat{\mathbf{m}}(\mathbf{r}) \cdot \mathbf{E}^b_I(\mathbf{r})\right]. \tag{2.9}$$

Following [4, 13], we can take into account that the Green's tensor $\widehat{\mathbf{G}}_E(\mathbf{r}_j \mid \mathbf{r})$ exhibits either singularity or a peak at the point where $\mathbf{r}_j = \mathbf{r}$. Therefore, the dominant contribution to the integral $\mathbf{G}_E[\widehat{\mathbf{m}}(\mathbf{r}) \cdot \mathbf{E}_I^b(\mathbf{r})]$ in Eq. (2.8) is from some vicinity of point $\mathbf{r}_j = \mathbf{r}$. Assuming also that the background field $\mathbf{E}_I^b(\mathbf{r})$ is slowly varying within domain D, we can rewrite Eq. (2.8) as

$$\mathbf{E}_I^a(\mathbf{r}_j) \approx \mathbf{G}_E[\widehat{\mathbf{m}}(\mathbf{r})] \cdot \mathbf{E}_I^b(\mathbf{r}_j), \tag{2.10}$$

where the tensor Green's operator $\mathbf{G}_E[\widehat{\mathbf{m}}(\mathbf{r})]$ is given by the formula

$$\mathbf{G}_E[\widehat{\mathbf{m}}(\mathbf{r})] = \iiint_D \widehat{\mathbf{G}}_E(\mathbf{r}_j \mid \mathbf{r}) \cdot \widehat{\mathbf{m}}(\mathbf{r}) dv. \tag{2.11}$$

Comparing Eqs. (2.5) and (2.10), we find that

$$\mathbf{E}_I^a(\mathbf{r}_j) \approx \widehat{\boldsymbol{\lambda}}(\mathbf{r}_j) \cdot \mathbf{E}_I^b(\mathbf{r}_j) \approx \mathbf{G}_E[\widehat{\mathbf{m}}(\mathbf{r})] \cdot \mathbf{E}_I^b(\mathbf{r}_j).$$

Therefore, the electrical reflectivity tensor can be determined from the solution of the minimization problem,

$$\left\| \widehat{\boldsymbol{\lambda}}(\mathbf{r}_j) \cdot \mathbf{E}_I^b(\mathbf{r}_j) - \mathbf{G}_E[\widehat{\mathbf{m}}(\mathbf{r})] \cdot \mathbf{E}_I^b(\mathbf{r}_j) \right\|_{L_2(D)} = \min. \tag{2.12}$$

Noting that

$$\begin{aligned} &\left\| \widehat{\boldsymbol{\lambda}}(\mathbf{r}_j) \cdot \mathbf{E}_I^b(\mathbf{r}_j) - \mathbf{G}_E[\widehat{\mathbf{m}}(\mathbf{r})] \cdot \mathbf{E}_I^b(\mathbf{r}_j) \right\|_{L_2(D)} \\ \leq &\left\| \widehat{\boldsymbol{\lambda}}(\mathbf{r}_j) - \mathbf{G}_E[\widehat{\mathbf{m}}(\mathbf{r})] \right\|_{L_2(D)} \left\| \mathbf{E}_I^b(\mathbf{r}_j) \right\|_{L_2(D)}, \end{aligned}$$

we can substitute another problem,

$$\left\| \widehat{\boldsymbol{\lambda}}(\mathbf{r}_j) - \mathbf{G}_E[\widehat{\mathbf{m}}(\mathbf{r})] \right\|_{L_2(D)} = \min, \tag{2.13}$$

for the minimization problem (2.12).

The solution of Eq. (2.13) gives us *a localized electrical reflectivity tensor*, $\widehat{\boldsymbol{\lambda}}(\mathbf{r})$, which is obviously source independent.

Note that in the framework of the LQL method, we can choose different forms of the reflectivity tensor. For example, we can introduce a scalar or diagonal reflectivity tensor. The choice of electrical reflectivity tensor is related to the physics of the problem and the accuracy and speed required in the computations. The interested reader can find the detailed analysis of the selection of the different types of electrical reflectivity tensor and related accuracy of the LQL approximation in [18].

We assume now that the anomalous parts of the electric, $\mathbf{E}^a(\mathbf{r}_j)$, and/or magnetic, $\mathbf{H}^a(\mathbf{r}_j)$, fields (generated by a transmitter with one or multiple positions) are measured

at a number of observation points, $\mathbf{r}_j$. Using the LQL approximations (2.8) and (2.9) for the observed fields, $\mathbf{d}$, we arrive at the following equation:

$$\mathbf{d}=\mathbf{G}_d\left[\widehat{\mathbf{m}}(\mathbf{r})\cdot\mathbf{E}^b(\mathbf{r})\right], \tag{2.14}$$

which is linear with respect to the material property tensor, $\widehat{\mathbf{m}}(\mathbf{r})$. In the last equation, $\mathbf{d}$ stands for the electric or magnetic field at the receivers, $\mathbf{E}$ or $\mathbf{H}$, and $\mathbf{G}_d$ denotes the Green's operators, $\mathbf{G}_E$ or $\mathbf{G}_H$, operating from the domain to the receivers.

We can solve the linear equation (2.14) with respect to $\widehat{\mathbf{m}}(\mathbf{r})$, which is source independent. This problem is solved by a standard least-squares optimization.

The reflectivity tensor, $\widehat{\boldsymbol{\lambda}}(\mathbf{r})$, is determined based on condition (2.13),which constitutes an important step of the LQL inversion. Knowing $\widehat{\boldsymbol{\lambda}}(\mathbf{r})$ and $\widehat{\mathbf{m}}(\mathbf{r})$, we can find $\Delta\sigma_{LQL}(\mathbf{r})$ from Eq. (2.7). Note that, in a general case, Eq. (2.7) should hold for any frequency, because the electrical reflectivity and the material property tensors are functions of frequency as well: $\widehat{\boldsymbol{\lambda}}=\widehat{\boldsymbol{\lambda}}(\mathbf{r},\omega)$, $\widehat{\mathbf{m}}=\widehat{\mathbf{m}}(\mathbf{r},\omega)$. In reality, however, it holds only approximately. Therefore, the conductivity, $\Delta\sigma_{LQL}(\mathbf{r})$, can be found by using the least-squares method of solving Eq. (2.7):

$$\left\|\widehat{\mathbf{m}}(\mathbf{r},\omega)-\Delta\sigma_{LQL}(\mathbf{r})\left(\widehat{\mathbf{I}}+\widehat{\boldsymbol{\lambda}}(\mathbf{r},\omega)\right)\right\|_{L_2(\omega)}=\min. \tag{2.15}$$

This inversion scheme can be used for a multi-source technique, because $\widehat{\boldsymbol{\lambda}}$ and $\widehat{\mathbf{m}}$ are source independent. It reduces the original nonlinear inverse problem to three linear inverse problems: the first (quasi-Born inversion) for tensor $\widehat{\mathbf{m}}$, the second for tensor $\widehat{\boldsymbol{\lambda}}$, and the third (correction of the result of the quasi-Born inversion) for the conductivity, $\Delta\sigma_{LQL}$.

2.3 The regularized inversion method

We can rewrite Eq. (2.14) using matrix notations:

$$\mathbf{d}=\mathbf{G}\mathbf{m}. \tag{2.16}$$

Here $\mathbf{m}$ is the vector-column of the modified material property tensor $\widehat{\mathbf{m}}$, $\mathbf{d}$ is the vector-column of the field data, and $\mathbf{G}$ is the matrix of the linear operator defined by Eq. (2.14).

The solution of the inverse problem is reduced to the inversion of linear system (2.16) with respect to $\mathbf{m}$ and then to computing $\widehat{\boldsymbol{\lambda}}$ using condition (2.13). After that, we find $\Delta\sigma_{LQL}$ as a least-squares solution of the optimization problem (2.15). Note that in the case of a single frequency observations, we still have to solve the optimization problem (2.15), if we consider the full electrical reflectivity and material property tensors. In a case of single frequency observations and a scalar electrical reflectivity tensor, optimization problem (2.15) is reduced to a simple algebraic equation.

Thus, by using the approximation in Eq. (2.5), one difficult non-linear inversion problem has been converted into three linear inversions. This approximation holds for low

conductivity contrasts and can produce accurate results, but in the general case it may introduce an unquantified error into the domain electric field which propagates into the modeled response of the conductivity distribution. In field exploration, it is important to know accurately where the errors between the predicted and observed data lie. Hence, rapidly and accurately modeling the true response of the body is paramount.

We use the re-weighted regularized conjugate gradient method with image focusing [10] for solving the system of the linear equations (2.16), which is based on the Tikhonov regularization technique [14]. We introduce the following parametric functional:

$$P^{\alpha}(\mathbf{m},\mathbf{d})=\|\mathbf{W}_d\mathbf{G}\mathbf{m}-\mathbf{W}_d\mathbf{d}\|^2+\alpha\|\mathbf{W}_m\mathbf{m}-\mathbf{W}_m\mathbf{m}_{apr}\|^2, \tag{2.17}$$

where $\mathbf{W}_d$ and $\mathbf{W}_m$ are some real weighting matrices of data and model parameters; $\mathbf{m}_{apr}$ is some *a priori* model, and $\|\cdots\|$ denotes the Euclidean norm in the spaces of data and models.

In the majority of practical applications, we assume that $\mathbf{W}_m=\mathbf{I}$, (where $\mathbf{I}$ is the identity matrix), but it also can be chosen arbitrarily. For example, it could be a matrix of first order or second order finite-difference differentiation to obtain a smooth solution. In particular, it was demonstrated in [14] that the recommended choice of the model parameter weighting matrix, $\mathbf{W}_m$, is the square root of the integrated sensitivity matrix according to

$$\mathbf{W}_m=\mathbf{diag}(\mathbf{G}^*\mathbf{G})^{1/4}, \tag{2.18}$$

where the asterisk $(*)$ denotes a transposed complex conjugate matrix.

Following [14], we solve our problem in the space of weighted parameters. We introduce a vector of weighted model parameters

$$\mathbf{m}_w=\mathbf{W}_m\mathbf{m}.$$

The original vector of model parameters is given by the inverse transformation

$$\mathbf{m}=\mathbf{W}_m^{-1}\mathbf{m}_w.$$

We also introduce a weighted forward operator

$$\mathbf{G}_w=\mathbf{G}\mathbf{W}_m^{-1}.$$

Now we can rewrite the functional $P^{\alpha}(\mathbf{m}_w,\mathbf{d})$ with matrix notations

$$\begin{aligned}P^{\alpha}(\mathbf{m}_w,\mathbf{d})=&(\mathbf{W}_d^*\mathbf{G}_w^*\mathbf{m}_w^*-\mathbf{W}_d\mathbf{d}^*)^T(\mathbf{W}_d\mathbf{G}_w\mathbf{m}_w-\mathbf{W}_d\mathbf{d})\\&+\alpha(\mathbf{m}_w^*-\mathbf{m}_{w,apr}^*)^T(\mathbf{m}_w-\mathbf{m}_{w,apr}),\end{aligned}$$

where superscript 'T' denotes transposition, and asterisk $*$ denotes a complex conjugate.

According to the basic principles of the regularization method, we have to find a quasi-solution to the inverse problem for the model, $\mathbf{m}_{w,\alpha}$, minimizing the parametric functional,

$$P^{\alpha}(\mathbf{m}_{w,\alpha},\mathbf{d})=\min.$$

The most common approach to minimization of the parametric functional $P^{\alpha}(\mathbf{m},\mathbf{d})$ is based on using gradient-type methods. For example, the regularized conjugate gradient (RCG) algorithm of the parametric functional minimization in the case of the minimum norm stabilizer can be summarized as follows [18]:

$$\begin{aligned}
&\mathbf{r}_n=\mathbf{G}_w\mathbf{m}_{w,n}-\mathbf{d},\ \mathbf{l}_n=\mathbf{l}(\mathbf{m}_{w,n})=\mathbf{Re}(\mathbf{G}_w^{\star}\mathbf{W}_d^{\star}\mathbf{W}_d\mathbf{r}_n)+\alpha(\mathbf{m}_{w,n}-\mathbf{m}_{w,apr}),\\
&\beta_n=\|\mathbf{l}_n\|^2/\|\mathbf{l}_{n-1}\|^2,\ \tilde{\mathbf{l}}_n=\mathbf{l}_n+\beta_n\tilde{\mathbf{l}}_{n-1},\ \tilde{\mathbf{l}}_0=\mathbf{l}_0,\\
&k_n=(\tilde{\mathbf{l}}_n,\mathbf{l}_n)/\left\{\left\|\mathbf{W}_d\mathbf{G}_w\tilde{\mathbf{l}}_n\right\|^2+\alpha\left\|\tilde{\mathbf{l}}_n\right\|^2\right\},\\
&\mathbf{m}_{w,n+1}=\mathbf{m}_{w,n}-k_n\tilde{\mathbf{l}}_n,
\end{aligned}\tag{2.19}$$

where k_n is a length of the iteration step, and $\mathbf{l}_n$ is the gradient direction computed using the adjoint operator, $\mathbf{G}_w^{\star}$.

The regularization parameter α is determined from the misfit condition:

$$\|\mathbf{W}_d\mathbf{G}_w\mathbf{m}_{w,\alpha}-\mathbf{W}_d\mathbf{d}\|=\delta,\tag{2.20}$$

where δ is some *a priori* estimation of the level of the "weighted" noise of the data:

$$\|\mathbf{W}_d\delta\mathbf{d}\|=\delta.\tag{2.21}$$

We apply the *adaptive* regularization method. The regularization parameter α is updated in the process of the iterative inversion as follows:

$$\alpha_n=\alpha_1 q^{n-1};\quad n=1,2,\cdots;\quad 0<q<1.\tag{2.22}$$

In order to avoid divergence, we begin with an initial value of α_1, which can be obtained as a ratio of the misfit functional and the stabilizer for an initial model, then reduce α_n according to Eq. (2.22) on each subsequent iteration and continuously iterate until the misfit condition is reached:

$$r_{n0}^{w}=\|\mathbf{r}_{n0}^{w}\|=\|\mathbf{W}_d(\mathbf{G}(\mathbf{m}_{\alpha_{n0}})-\mathbf{d})\|/\|\mathbf{W}_d\mathbf{d}\|=\delta,\tag{2.23}$$

where r_{n0}^{w} is the normalized weighted residual, and δ is the relative level of noise in the weighted observed data.

Parameter q controls the rate of decrease of the regularization parameter α_n in the process of inversion. This parameter is usually selected within an interval [0.5; 0.9].

2.4 Solution to the domain equation

The rigorous stage of the inversion algorithm is based on the iterative solution of the field and domain equations. Determining accurate predicted data once the electric field is known is a straight forward process requiring only matrix multiplication. Rapidly calculating the true domain electric field is more challenging. In order to ensure the

convergence of the corresponding iterative process, we use the contraction form of the domain equation [7]:

$$a\mathbf{E}^a+b\mathbf{E}^b=\mathbf{G}_E^m\left[b(\mathbf{E}^a+\mathbf{E}^b)\right], \tag{2.24}$$

where

$$a=\frac{2\sigma_b+\Delta\sigma}{2\sqrt{\sigma_b}}, \quad b=\frac{\Delta\sigma}{2\sqrt{\sigma_b}}, \tag{2.25}$$

and modified Green's operator $\mathbf{G}_E^m(\mathbf{x})$ is defined as a linear transformation of the original electric Green's operator:

$$\mathbf{G}_E^m(\mathbf{x})=\sqrt{\sigma_b}\mathbf{G}_E(2\sqrt{\sigma_b}\mathbf{x})+\mathbf{x}. \tag{2.26}$$

The advantage of Eq. (2.24) over the conventional domain equation is that the L_2 norm of the modified Green's operator is always less than or equal to one [9]:

$$\|\mathbf{G}_E^m\|\leq 1. \tag{2.27}$$

Eq. (2.24) can be rewritten with respect to the product of a and the total electric field $\mathbf{E}$, using simple algebraic transformations:

$$\widetilde{\mathbf{E}}+(b-a)\mathbf{E}^b=\widetilde{\mathbf{E}}-\sqrt{\sigma_b}\mathbf{E}^b=\mathbf{G}_E^m\left[ba^{-1}\widetilde{\mathbf{E}}\right], \tag{2.28}$$

where $\widetilde{\mathbf{E}}$ is the scaled electric field

$$\widetilde{\mathbf{E}}=a\mathbf{E}. \tag{2.29}$$

Finally, we can present Eq. (2.28) in the form

$$\widetilde{\mathbf{E}}=\mathbf{C}^m\left(\widetilde{\mathbf{E}}\right)=\mathbf{G}_E^m\left[ba^{-1}\widetilde{\mathbf{E}}\right]+\sqrt{\sigma_b}\mathbf{E}^b. \tag{2.30}$$

In this equation, operator $\mathbf{C}^m\left(\widetilde{\mathbf{E}}\right)$ is a contraction operator for any lossy medium [14]:

$$\left\|\mathbf{C}^m\left(\widetilde{\mathbf{E}}^{(1)}-\widetilde{\mathbf{E}}^{(2)}\right)\right\|\leq k\left\|\widetilde{\mathbf{E}}^{(1)}-\widetilde{\mathbf{E}}^{(2)}\right\|, \tag{2.31}$$

where $\|\cdots\|$ is the L_2 norm, $k<1$, and $\widetilde{\mathbf{E}}^{(1)}$and $\widetilde{\mathbf{E}}^{(2)}$ are any two different solutions.

Substituting Eq. (2.26) into (2.30), we have:

$$\widetilde{\mathbf{E}}=\sqrt{\sigma_b}\mathbf{G}_E\left(2\sqrt{\sigma_b}ba^{-1}\widetilde{\mathbf{E}}\right)+ba^{-1}\widetilde{\mathbf{E}}+\sqrt{\sigma_b}\mathbf{E}^b. \tag{2.32}$$

Taking into account Eq. (2.25) for coefficients a and b, we can rewrite Eq. (2.32) in equivalent form:

$$\widetilde{\mathbf{E}}=2\sqrt{\sigma_b}\mathbf{G}_E\left[\sqrt{\sigma_b}\beta\widetilde{\mathbf{E}}\right]+\beta\widetilde{\mathbf{E}}+\sqrt{\sigma_b}\mathbf{E}^b, \tag{2.33}$$

where we have introduced a new parameter, β, as:

$$\beta=ba^{-1}=\frac{\Delta\sigma}{\Delta\sigma+2\sigma_b}.$$

Eq. (2.33) is solved using the complex conjugate minimal residual (CGMRES) method [14]. The only requirement for convergence of this algorithm is that the matrix must be absolutely positively determined. In IE forward modeling, due to the energy inequality, the matrix always has this property [7].

2.5 Rigorous inversion

We now apply the above solution to the domain equation for rigorous inversion. The first step is to rigorously determine the electric field inside the domain from the LQL conductivity distribution. To accomplish this, we use the electric field from LQL (Eq. (2.6), with $\widehat{\lambda}$ found during inversion) as an initial guess:

$$\mathbf{E}=\mathbf{E}^a_{LQL}+\mathbf{E}^b\approx\left(\widehat{\lambda}+\widehat{\mathbf{I}}\right)\cdot\mathbf{E}^b\left(\mathbf{r}_j\right).$$

A preconditioned form of the domain equation, which accelerates convergence, is used to calculate the electric field [7]:

$$\widetilde{\mathbf{E}}^{(0)}_I=2\sqrt{\sigma_b}\mathbf{G}_E\left[\sqrt{\sigma_b}\beta\widetilde{\mathbf{E}}^{(0)}_I\right]+\beta\widetilde{\mathbf{E}}^{(0)}_I+\sqrt{\sigma_b}\mathbf{E}^b_I, \tag{2.34}$$

where

$$\beta=\frac{\Delta\sigma_{LQL}}{\Delta\sigma_{LQL}+2\sigma_b}. \tag{2.35}$$

The transformed electric field $\widetilde{\mathbf{E}}^{(0)}_I$ is simply

$$\widetilde{\mathbf{E}}^{(0)}_I=a\mathbf{E}^{(0)}_I, \tag{2.36}$$

where

$$a=\frac{2\sigma_b+\Delta\sigma_{LQL}}{2\sqrt{\sigma_b}}. \tag{2.37}$$

In this stage, Eq. (2.34) is solved to a relatively low accuracy (10%). This is much faster than requiring the more common forward modeling accuracy of 10^{-6}, yet still accurate enough to gauge the error in the LQL inversion.

Once the electric field inside the domain has been attained, the true data predicted from the LQL conductivity distribution is given by:

$$\begin{aligned}\mathbf{H}^{pr(LQL)}_I\left(\mathbf{r}_j\right)&=\iiint_D\widehat{\mathbf{G}}_H\left(\mathbf{r}_j\,|\,\mathbf{r}\right)\cdot\Delta\sigma_{LQL}\left(\mathbf{r}\right)\mathbf{E}^{(0)}_I\left(\mathbf{r}\right)dv\\&=\mathbf{G}_H\left[\Delta\sigma_{LQL}\mathbf{E}^{(0)}_I\right].\end{aligned} \tag{2.38}$$

Note that the Green's operator $\mathbf{G}_H$ is the same as in Eq. (2.4). We can estimate the accuracy of our LQL inversion by computing the normalized misfit:

$$\delta_{LQL}=\frac{||\mathbf{H}^{pred}-\mathbf{H}^{obs}||}{||\mathbf{H}^{obs}||}. \tag{2.39}$$

We finish the inverse process if the error is less than some predetermined amount. Otherwise we can apply the inversion iteratively.

To begin the rigorous inversion, we use the updated field $\mathbf{E}_I^{(0)}(\mathbf{r})$ to find an updated conductivity $\Delta\sigma^{(1)}(\mathbf{r})$ from the equation:

$$\begin{aligned}\mathbf{H}_I^a(\mathbf{r}_j) &= \iiint_D \widehat{\mathbf{G}}_H(\mathbf{r}_j\,|\,\mathbf{r})\cdot\Delta\sigma^{(1)}(\mathbf{r})\mathbf{E}_I^{(0)}(\mathbf{r})\,dv \\ &= \mathbf{G}_H\left[\Delta\sigma^{(1)}\mathbf{E}_I^{(0)}\right], \quad I=1,2,\cdots,N. \end{aligned} \tag{2.40}$$

We solve the inverse problem (2.40) using the re-weighted regularized conjugate gradient (RRCG) minimization outlined in the previous section. This process is relatively fast, since we assume the operator is linear and therefore there is no need to compute a Jacobian (Frechet derivative matrix). However, as the model parameters change, the electric field, and hence the operator, becomes approximate and we must update it. The criteria for updating the electric field are two fold:

1. When the misfit in the inversion decreases a predetermined amount, or
2. When a certain number of RRCG iterations have been reached.

When one of these conditions is met, we use the new conductivity distribution, $\Delta\sigma^{(1)}$, to update the electric field, $\mathbf{E}^{(1)}(\mathbf{r})$, with the integral expression using CGMRES:

$$\tilde{\mathbf{E}}_I^{(1)} = \beta\tilde{\mathbf{E}}_I^{(1)} + 2\sqrt{\sigma_b}\mathbf{G}_E[\sqrt{\sigma_b}\beta\tilde{\mathbf{E}}_I^{(1)}] + \sqrt{\sigma_b}\tilde{\mathbf{E}}^b, \tag{2.41}$$

where

$$\beta = \frac{\Delta\sigma^{(1)}}{\Delta\sigma^{(1)}+2\sigma_b}. \tag{2.42}$$

The initial guess for the electric field is $\mathbf{E}_I^{(0)}$. Using the previous electric field as a starting point greatly reduces the number of iterations needed to find the next electric field to the required accuracy.

For the model with the conductivity $\Delta\sigma^{(1)}(\mathbf{r})$ we can calculate the predicted anomalous magnetic field $\mathbf{H}_I^{pr(1)}(\mathbf{r}_j)$ based on the equation:

$$\mathbf{H}_I^{pr(1)}(\mathbf{r}_j) = \mathbf{G}_H\left[\Delta\sigma^{(1)}\mathbf{E}_I^{(1)}\right]. \tag{2.43}$$

We also can estimate the accuracy of this solution by computing the normalized misfit.

This iterative process of updating the domain equation and then inverting the field equation continues. The accuracy to which the electric field is computed depends on the misfit of the inversion. Using this method, we require low accuracy in the initial iterations to speed the process, but as the inversion converges the forward operator is calculated to

greater accuracy. In step (k), we find an updated conductivity $\Delta\sigma^{(k)}(\mathbf{r})$ from the equation using the RRCG inversion:

$$\begin{aligned}\mathbf{H}_I^a(\mathbf{r}_j) &= \iiint_D \widehat{\mathbf{G}}_H(\mathbf{r}_j\,|\,\mathbf{r})\cdot\Delta\sigma(\mathbf{r})\,\mathbf{E}_I^{(k-1)}(\mathbf{r})\,dv \\ &= \mathbf{G}_H\left[\Delta\sigma\mathbf{E}_I^{(k-1)}\right], \quad I=1,2,\cdots,N. \end{aligned} \tag{2.44}$$

The field $\mathbf{E}_I^{(k-1)}(\mathbf{r})$ is precomputed using the equation

$$\tilde{\mathbf{E}}_I^{(k-1)} = \beta\tilde{\mathbf{E}}_I^{(k-1)} + 2\sqrt{\sigma_b}\mathbf{G}_E[\sqrt{\sigma_b}\beta\tilde{\mathbf{E}}_I^{(k-1)}] + \sqrt{\sigma_b}\tilde{\mathbf{E}}^b, \tag{2.45}$$

where

$$\beta_{k-1} = \frac{\Delta\sigma^{(k-1)}}{\Delta\sigma^{(k-1)} + 2\sigma_b}.$$

We use the updated conductivity $\Delta\sigma^{(k)}$ to find the updated electric field $\mathbf{E}_I^{(k)}(\mathbf{r})$ from Eq. (2.45). Then we compute the predicted anomalous magnetic field $\mathbf{H}_I^{pr(k)}(\mathbf{r}_j)$ at iteration k:

$$\mathbf{H}_I^{pr(k)}(\mathbf{r}_j) = \mathbf{G}_H\left[\Delta\sigma^{(k)}\mathbf{E}_I^{(k)}\right]. \tag{2.46}$$

The iterative process continues until we reach a predetermined error or number of iterations. The next sections show applications of this method to both synthetic and field data.

3 Inversion of synthetic AEM data

To test the inversion, we simulate the low frequency channels from a typical DIGHEM airborne survey [3] over two test bodies that are electromagnetically coupled. The synthetic model and survey are shown in Fig. 1. Six flight lines in the x direction are synthesized at 30 m bird height with 100 m line spacing and data collected every 50 m along line. The responses of two coplanar (7200 and 900 Hz) channels and one coaxial (900 Hz) channel with 8 m transmitter-receiver separations are calculated.

The inversion domain was divided into 27 cells in the x and y directions and 7 in the z direction, yielding approximately 5100 cells. We simultaneously invert all three channels for a total of 198 sounding locations. The AEM data were computed by the IE forward modeling code INTEM3D and contaminated by Gaussian noise with a standard deviation of 1.5 ppm, which is a typical value for an AEM survey. This corresponds to between 5% and 50% noise, depending on the channel.

The inversion was run initially with LQL method to obtain a fast image of the body (see Fig. 2). The resistivity is overestimated, especially for the lower body, but the general locations of the bodies are delineated. At the completion of the LQL inversion, a fast

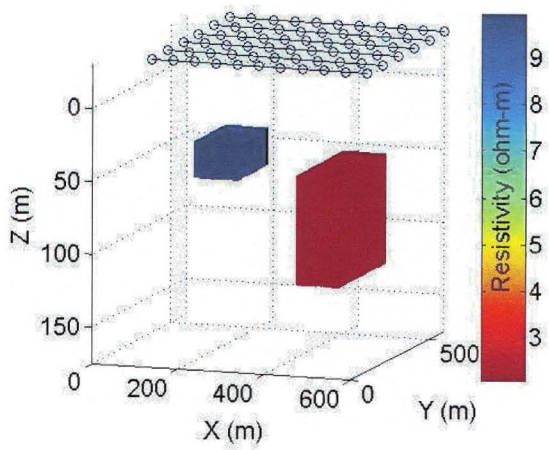

Figure 1: The geoelectric model with two conductive bodies and AEM survey design. The upper body is 10 ohm-m, and the lower body is 2 ohm-m. They are imbedded in a 100 ohm-m halfspace. The flight lines are shown as blue lines with circles for sounding locations.

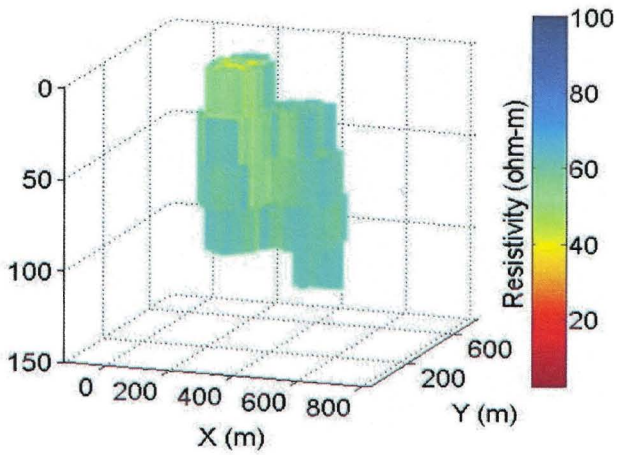

Figure 2: LQL inversion results. The resistivity values greater than 60 ohm-m are removed from the view. The locations of the bodies are evident, but the resistivity is overestimated. Note also that the lateral extents of this figure are greater than that of the figure showing the true bodies. This reflects padding at the edges of the inversion domain.

check is performed on the accuracy of the solution by rigorously calculating the domain electric field. The LQL predicted data matches the observed data well, but the rigorously predicted data to the LQL inverse solution shows there is still room for improvement

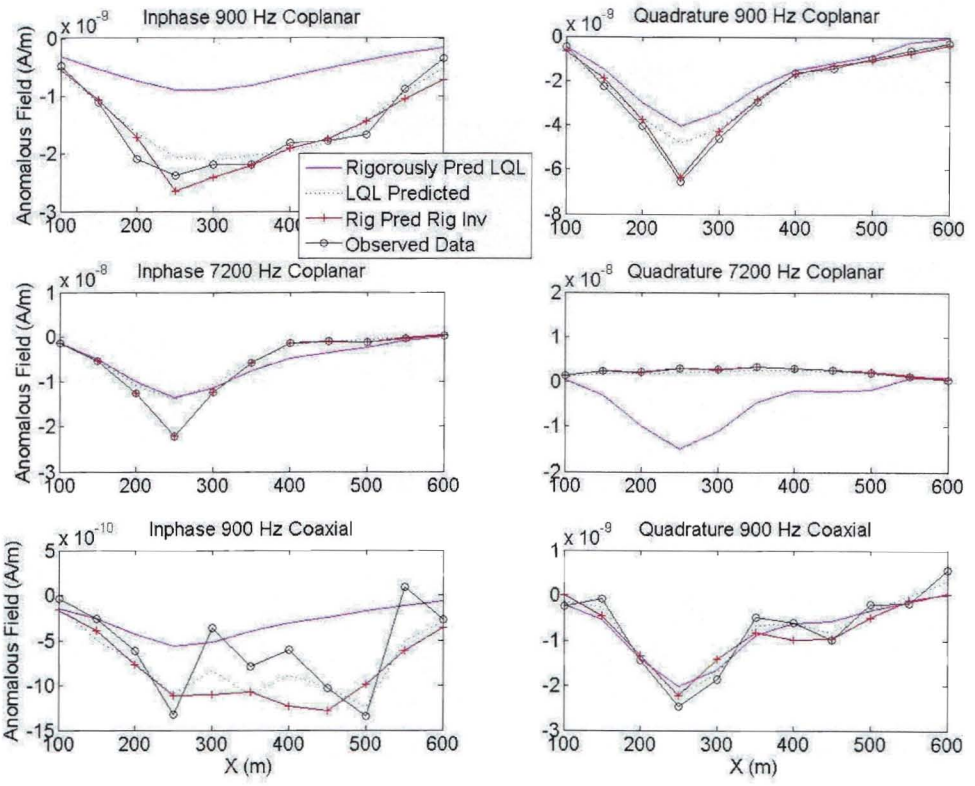

Figure 3: Predicted and observed data for a synthetic AEM survey. The data shown are along a profile at y=300 m. The curve "Rigorously Pred LQL" corresponds to the rigorously predicted data for the LQL solution. "LQL Predicted" curve is the approximately predicted data to the LQL solution. The line marked as "Rig Pred Rig Inv" shows the final predicted data. Also shown are the synthetic data. Note the large error introduced into the observed data of the coaxial channel using 1.5 ppm error.

in the conductivity distribution (Fig. 3). The true response of the 7200 Hz quadrature channel differs significantly from the approximate solution, but the rest of the channels are in reasonable agreement.

The rigorous inversion uses a reweighted conjugate gradient scheme starting with the LQL result as the initial model. The error level is set to 1.5 ppm for all data points. The rigorous inversion result is shown in Fig. 5. This inverse image is much improved over the LQL inversion, and the true normalized misfit is 13% (see Fig. 4). The bodies are shown to be separated and in their proper positions. The conductivity of the lower body is slightly underestimated and a hole appears in the center. The rigorous predicted data properly fits the observed data to the given noise levels (see Fig. 3). One can see this inversion is accurate and robust in the presence of noisy data.

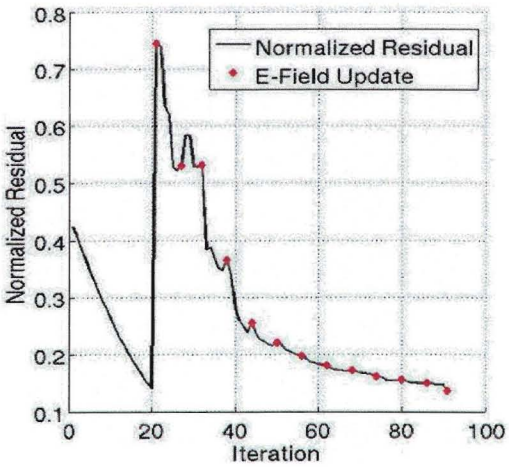

Figure 4: Normalized misfit and electric field updates as a function of iteration. Note the LQL inversion runs until it reaches the noise level in the data at iteration 20. The rigorous inversion then continues through the remaining iterations.

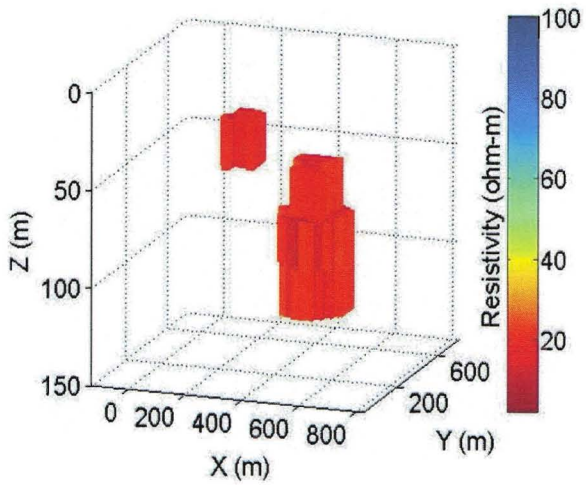

Figure 5: Rigorous inversion results for a synthetic airborne survey. The resistivity values greater than 20 ohm-m are removed from the view. The conductive bodies are now in the proper location and the resistivity is estimated much better than in the LQL result.

4 Inversion of AEM over a Kimberlite Pipe

4.1 Geologic setting

The survey data we have applied our inversion algorithm to is from the Ekati Diamond Mine, Canada. The target is a kimberlite pipe, which is the most common diamond bear-

Table 1: Data channels used for inversion.

Frequency (Hz)	Component	Estimated Error (ppm)
871	Coplanar	2.5
5834	Coaxial	10
7166	Coplanar	5

ing ore. Kimberlite pipes are an ultrabasic intrusion which are nearly circular and narrow with depth. The kimberlite material typically weathers into clays more rapidly than the surrounding rock. These clays are conductive and provide a target for EM methods [8]. The location in question has been glacially scoured, which has preferentially removed part of the weathered clay cap and left behind a lake.

4.2 Survey and inversion parameters

This survey was performed with the DIGHEM system consisting of 5 channels. We select three frequencies (see Table 1) for the test of our inversion code. The error in each channel was assigned after [5]. The original survey had very dense measurements, but for our inversion we used only every 100th data point giving a total of 34 soundings per channel. The flight height was approximately 25 m above ground level, and the transmitter-receiver separation was 7.98 m. The observed and predicted data are shown in Fig. 6.

The inversion domain contained 116 cells in the x direction, 108 in the y direction and 24 in the z direction, all linearly spaced, for approximately 300,000 total cells. The inversion domain extended from -200 m to 1200 m in the x, -200 m to 1100 m in the y, and 0 m to 300 m in the z direction. The model discretization was chosen after running multiple inversions with varying cell sizes. These sizes varied from $50\times50\times25$ m^3 to the $12\times12\times12$ m^3 we have chosen to show. Once the cells were smaller than $20\times20\times20$ m^3, the results of the inversion did not vary appreciable with decreasing cell size.

4.3 Inversion results

First, a one dimensional inversion was performed to find a layered earth background model. The best simple 1-D model was a homogenous halfspace with a resistivity of 3500 ohm-m. This model was used for the 3-D inversion scheme, as outlined above. The LQL inversion was run first to obtain a fast image. The final misfit in the predicted data from LQL after 17 iterations is 25%, but the true error in the solution as rigorously calculated using the scheme is 110%. Note that the geometry of the kimberlite was well resolved with the LQL inversion, but the conductivity distribution was highly overestimated in this case, causing a very large response and the large misfit.

We then use the LQL result as a starting model and followed the rigorous inversion algorithm to further delineate the model. The rigorous inversion runs for an additional 740 iterations giving a final rigorous misfit of 25%.

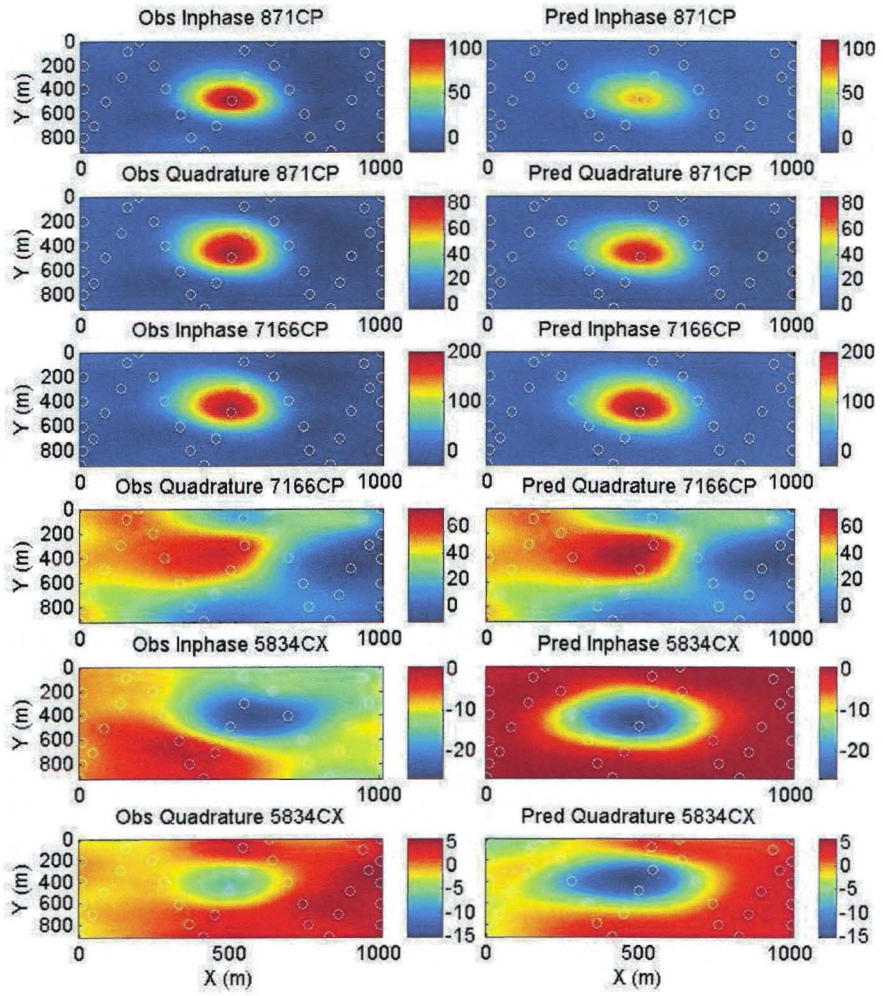

Figure 6: Observed and predicted AEM data over a kimberlite pipe. The observed data are on the left, and the predicted are on the right. The circles indicate data sounding locations used for the inversion. The various channels used are as labeled. Notice that the coaxial channel visually has the poorest fit, but the noise level in this channel was set to 10 ppm and the total anomaly is around 25 ppm. All other channels show a very good fit between the observed data and the data predicted from the inverse model.

The results from this rigorous inversion, along with the true kimberlite position, provided by BHP Billiton are shown in Fig. 7. This position is derived from extensive drilling, the lake bathymetry, and other geophysical methods (Dr. R. Ellis, personal communication). Our inversion result compares very favorably to this model. The model is strictly geometric; we do not have conductivity information. We should emphasize,

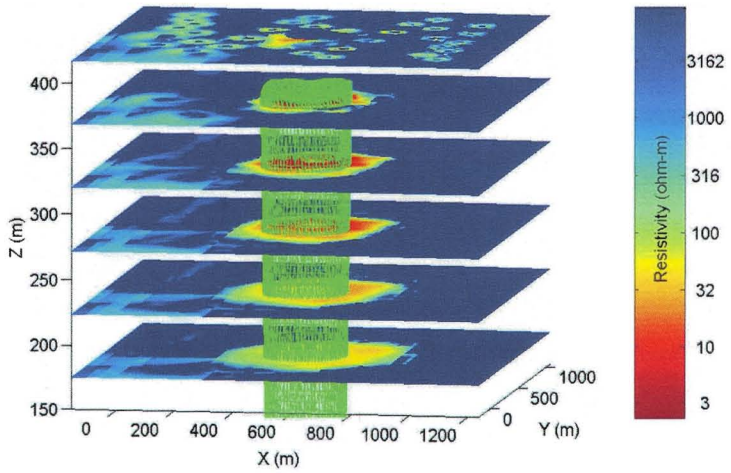

Figure 7: The result of rigorous inversion for practical AEM data collected over a kimberlite pipe. The true kimberlite position provided by BHP Billiton is overlain as the green mesh.

Table 2: Inversion times and misfits.

	Green's Tensors	LQL	Checking LQL	Rigorous Inversion	Total
Time	15 min	3 min	25 min	8.25 hours	9 hours
Number of Iterations	NA	17	NA	740	757
Percent Misfit	NA	25	110	25	25

however, that we did not have and we did not use information about the true position of the kimberlite pipe in our inversion. Notice the top of the kimberlite is very well resolved, with both the depth and diameter close to the true model. The conductivity is also assumed to be accurate, as wet clays typically have values around to 20 Ohm-m [12]. The model becomes slightly more diffuse at depth due to a lack of resolution. In addition, the resistivity becomes larger below the 150 m cross-section. This is most likely a combination of decaying resolution and the kimberlite becoming less weathered at depth and hence less conductive. There are also some artifacts below each transmitter position indicating the noise level in the data may have been slightly underestimated and some noise was fit.

The total inversion time on a 2.4 GHz AMD 64 processor with 4 Gb of RAM was 9 hours. The times of each stage are broken down in Table 2. The maximum ram used was 2.5 Gb.

The method presented here provides a rigorous solution allowing an accurate fit to the data, while still being reasonably fast.

5 Conclusion

In this paper we have demonstrated that the contraction integral equation method of solving Maxwell's equations can be successfully used for interpretation of geophysical EM data in complex geoelectrical structures. We have extended the method of AEM data interpretation based on the LQL approximation by adding a rigorous stage of inversion. This rigorous stage includes a rapid and stable solution to electric field equation by using the complex generalized minimum residual to solve a preconditioned form of the domain equation. Using the electric field from the previous inversion iteration reduces the number of CGMRES iterations needed to accurately calculate a new field and greatly speeds the inversion process. The rigorous 3-D solution to the AEM interpretation problem now is feasible on a single PC.

6 Acknowledgments

Dr. Robert Ellis of BHP Billiton graciously provided field data for the field example and the geologic model. We also appreciate the comments of Dr. Bryan Travis and one anonymous reviewer which improved the clarity of the manuscript.

We are thankful to Dr. Alex Gribenko of CEMI, University of Utah, for his contribution in the development of the iterative inversion code.

The authors acknowledge the support of the University of Utah Consortium for Electromagnetic Modeling and Inversion (CEMI), which includes BAE Systems, Baker Atlas Logging Services, BGP, China National Petroleum Corporation, BHP Billiton World Exploration Inc., Centre for Integrated Petroleum Research, EMGS, ENI S.p.A., Exxon Mobil Upstream Research Company, INCO Exploration, Information Systems Laboratories, MTEM, Newmont Mining Co., OHM Inc., Norsk Hydro, Petrobras, Rio Tinto, Russian Research Center, Rocksource, Schlumberger, Shell International Exploration and Production Inc., Statoil, Sumitomo Metal Mining Co., and Zonge Engineering and Research Organization.

References

[1] R. G. Ellis, Inversion of airborne electromagnetic data, SEG Technical Program Expanded Abstracts, 17(1) (1998), 2016-2019.

[2] C. G. Farquharson, D. W. Oldenburg and P. S. Routh, Simultaneous 1-D inversion of loop-loop electromagnetic data for magnetic susceptiblility and eletrical conductivity, Geophysics, 68(6) (2003), 1857-1869.

[3] Fugro, Fugro website, 2005, http://www.fugroairborne.com.au

[4] T. M. Habashy, R. W. Groom and B. R. Spies, Beyond the Born and Rytov approximations–a nonlinear approach to electromagnetic scattering, J. Geophys. Res., 98(B2) (1993), 1759-1775.

[5] G. Hodges, Technical notes–helicopter electromagnetics, http://www.fugroairborne.com.au, 2001.

[6] H. Huang and D. C. Fraser, The differential parameter mapping for multifrequency airborne resisitivty mapping, Geophysics, 61(1) (1996), 100-109.
[7] G. Hursán and M. S. Zhdanov, Contraction integral equation method in three-dimensional electromagnetic modeling, Radio Sci., 37(6) (2002), 1089.
[8] J. C. Macnae, Kimberlites and exploration geophysics, Geophysics, 44 (1979), 1395-1416.
[9] O. V. Pankratov, A. V. Kuvshinov and D. B. Avdeev, High-performance three-dimensional electromagnetic modeling using modified Neumann series. Anisotropic case, J. Geomagn. Geoelectr., 49 (1997), 1541-1547.
[10] O. Portnaiguine and M. S. Zhdanov, Focusing geophysical inversion images, Geophysics, 64(3) (1999), 874-887.
[11] K.-P. Sengpiel and B. Siemon, Advanced inversion methods for airborne electromagnetic exploration, Geophysics, 65(6) (2000), 1983-1992.
[12] W. M. Telford, L. P. Geldart and R. E. Sheriff, Applied Geophysics, 2nd Ed., Cambridge University Press, New York, 1990.
[13] C. Torres-Verdin and T. M. Habashy, Rapid 2.5-dimensional forward modeling and inversion via a new nonlinear scattering approximation, Radio Sci., 29 (1994), 1051-1079.
[14] M. S. Zhdanov, Geophysical inverse theory and regularization problems, in: Methods in Geochemistry and Geophysics, Vol. 36, Elsevier, San Francisco, 2002.
[15] M. S. Zhdanov and A. Chernyavskiy, Rapid three-dimensional inversion of multi-transmitter electromagnetic data using the spectral Lanczos decomposition method, Inverse Probl., 20 (2004), S233-S256.
[16] M. S. Zhdanov and S. Fang, 3-D quasi-linear electromagnetic inversion, Radio Sci., 31 (1996), 741-754.
[17] M. S. Zhdanov and S. Fang, Quasi-linear approximation in 3-D EM modeling, Geophysics, 61 (1996), 646-665.
[18] M. S. Zhdanov and E. Tartaras, Three-dimensional inversion of multitransmitter electromagnetic data based on the localized quasi-linear approximation, Geophys. J. Int., 148 (2002), 506-519.